Band structure effects on the charge exchange processes in H+ colliding with a Cu(111) surface.

Journal:	*The Journal of Physical Chemistry*
Manuscript ID	Draft
Manuscript Type:	Article
Date Submitted by the Author:	n/a
Complete List of Authors:	Quintero Riascos, Vanessa; Instituto de Física del Litoral (CONICET - UNL) Tacca, Marcos; Instituto de Física del Litoral (CONICET - UNL) Vidal, Ricardo; Instituto de Física del Litoral (CONICET - UNL) Gonzalez, Cesar; Instituto de Ciencia de Materiales de Madrid, Goldberg, Edith; Instituto de Física del Litoral (CONICET - UNL) Bonetto, Fernando; Instituto de Física del Litoral (CONICET-UNL),

Band structure effects on the charge exchange processes in H$^+$ colliding with a Cu(111) surface.

V. Quintero Riascos[1], M. Tacca[1], R. Vidal[1,2], C. Gonzalez[3], E.C. Goldberg[1,2] and F. Bonetto[1,2]

[1]Instituto de Física del Litoral (CONICET-UNL), Güemes 3450, S3000GLN Santa Fe, Argentina.

[2]Departamento de Física, Facultad de Ing. Química, Universidad Nacional del Litoral, Santiago del Estero 2829, S3000AOM Santa Fe, Argentina.

[3]Departamento de Física Teórica de la Materia Condensada and Condensed Matter Physics Center (IFIMAC), Facultad de Ciencias, Universidad Autónoma de Madrid, 28049 Madrid, Spain.

1

ABSTRACT

The low energy ion scattering (LEIS) technique was used to experimentally determine the formation of positive and negative ions in the scattering of protons by a Cu(111) surface for a large scattering angle in the backscattering configuration and a wide range of incoming energies (2 to 8keV). Two different collisional geometries were analyzed for a 135° fixed scattering angle: 45°/90° and 67.5°/67.5° incoming/exit angles measured with respect to the target surface. The total fraction of backscattered ions ranges from 10% to 25% and a peculiarly high yield of negative ions, which always exceeds that of positive ions, was detected for the whole energy range analyzed. A strong dependence of the measured ion fractions with the geometrical conditions was experimentally found. On the theoretical side, a first principles quantum-mechanical formalism that takes into account the three possible final charge states of the H^+ in a correlated way and the fine details of the band structure of Cu(111) surface, was applied to describe the charge transfer processes involved in the experimental situation. The theoretical calculation leads to a non-monotonous dependence with the incoming energy that properly describes the experimental results, especially the negative ion fraction in the specular collisional geometry. The oscillatory behavior predicted by the theory in the range of low energies is a clear evidence of the charge exchange between localized states, that is the situation related with the presence of the surface state immersed in the L-gap present in Cu(111) surface. The positive ion fraction is discussed for the first time for this collisional system. The differences found between the measurements and the theory seem to indicate that the neutralization to excited states, and also the formation of excited negative hydrogen ions, are possible charge exchange channels in the dynamic process analyzed.

[*]corresponding author. Tel.: +54-342-4559175; Fax: +54-342-4550944

E-mail address: bonetto@santafe-conicet.gov.ar

1. INTRODUCTION

Electron transfer between atoms is a fundamental process that has been studied since the beginning of atomic physics and chemistry. Particularly, the charge transfer during collisions between ions and solid targets constitutes one of the basis for the analysis of surfaces [1,2]. Charge transfer processes depend on three main factors: i- the range of the projectile energies; ii- the scattering geometry and iii- the projectile-target surface system under study. Although experimentally independent, the influence of these three factors on charge exchange processes is interconnected. For example, the final ion fraction dependence on the incoming energy strongly depends on the experimental geometry and the system under study. Different combinations of these factors could lead to higher or lower ion fractions and to a prevalent positive or negative ion formation.

The final charge state of a projectile ion following a collision with a surface is relevant to both, fundamental and applied research. The latter is mainly related to technological applications in plasma-wall interaction for fusion devices [3,4], heterogeneous catalysis [5], particle detectors [6,7] and film deposition [8]. Its basic interest mostly lies in the actual incomplete understanding of the physical mechanisms engaged in electronic transfer during dynamic processes; being so far an active topic of current research [9-16].

The formation of negative ions during the collision with metal surfaces has been extensively studied both, theoretically and experimentally [5-7,14-39]. Most of these studies were devoted to H$^-$ formation [5,7,15,18-25,27,30,31,33,36-39] due to its practical relevance in plasma physics, where a high formation of negative hydrogen ions after a collision with a given surface is required. To achieve this goal, the work function of the target surface (usually W(100) or Mo(001)) is generally lowered by different degrees of Cs coverage [18,38,40]. With this method, up to 80% of H$^-$ formation is obtained [38].

The physical mechanisms that control the charge transfer process when hydrogen ions collide with a copper surface had been investigated in the past [5,15,30,31,39]. However, only few of these articles offer experimental support [31,39], and none of them compare experimental positive and negative hydrogen final ion fractions in an ample range of energies.

3

Here we present experimental data of positive, negative and total final ion fractions of H^+ projectiles colliding with a Cu(111) surface for a wide range of energies (2keV – 8keV), a fixed scattering angle (135°) and two incident/exit angle combinations: 45°/90° and 67.5°/67.5°. A particularly high yield of negative ions is obtained when compared to that of positive ions in the whole energy range analyzed. In addition, the negative ion fractions obtained (up to 15%) are larger than those previously obtained in literature under slightly different experimental conditions [31].

The formation of negative ions in the scattering of protons by a highly oriented pyrolytic graphite surface (HOPG) has been experimentally and theoretically studied by our group in the same range of incoming energies and similar scattering geometries [36]. Back then, we arrived to an important conclusion: the uncertainty introduced by the proton velocity diminishes the effective electron-electron coulomb repulsion and invalidates the adiabatic shift of the ion levels. This conclusion, related mainly to the ion projectile and its range of incoming energies, still applies to the present collisional system. Therefore, the same theoretical proposal based on the Anderson model and a second order perturbation treatment of the electronic repulsion in the projectile atomic state [36] was used to describe the experimental data obtained in the present work. The different characteristics between the HOPG and Cu(111) surfaces will be then responsible for the differences found in the incoming energy ion fraction dependences in both surfaces. The presence of the localized surface state inside the L-gap, a distinctive feature of the Cu(111) surface, is expected to introduce a non-monotonous dependence on the incoming energy.

2. EXPERIMENTAL

The low-energy ion scattering (LEIS) technique [1,41] was employed to experimentally determine the final charge state of the hydrogen ions scattered by a copper surface. The equipment used essentially consists of an ultra-high vacuum (UHV) chamber (base pressure in the order of 10^{-9} mbar), an ion gun with a Wien filter that allows for mass selection of the projectile ion and a time-of-flight (TOF) spectrometer. Additionally, Auger and low energy electron diffraction (LEED) techniques are available in the same chamber.

The H^+ ions are generated in a discharge source (Colutron). Then, the ion beam is accelerated and mass analyzed using the velocity filter. The beam is next swept by applying a square-wave pulse voltage to a pair of deflection plates placed in front of a slit to create a pulsed ion beam. These pulses of H^+ ions impact the Cu(111) monocrystalline target.

The temporal (or energy) distributions of total H ions, H^+, H^- and H neutral atoms scattered off the sample surface are measured by TOF methods [42]. Concisely, the same trigger signal of the pulse generator plates is used as the start pulse for a multichannel scaler (Ortec, Microchannel Scaler-MCS). All the particles scattered by the sample that reach the detector generate a pulse that is collected in a specific time channel of the MCS. The distribution of the time of flight of the particles is then generated by the MCS and finally shown and recorded as a histogram (TOF spectrum) by a processor. To speed up the measurement of a given spectrum, the pulse generation rate was fixed at 3 kHz or 10 kHz depending on the intensity of the signal. That is, the more intense the signal, the lower the rate for pulse generation (higher time resolution in TOF spectrum).

The scattering angle θ was set in backscattering configuration to $\theta= 135°$. Two pairs of incoming (α) and exit (β) angles, measured with respect to the surface plane, were selected to perform charge transfer experiments: $\alpha/\beta= 45°/90°$ and $\alpha/\beta= 67.5°/67.5°$ (see Fig. 1). In the first case ($\alpha/\beta= 45°/90°$) the exit angle β matches the collisional geometry used in the theoretical model ($\alpha/\beta= 90°/90°$). The second geometrical setup chosen ($\alpha/\beta= 67.5°/67.5°$), fulfills the specular condition present in the theoretical model. Measurements were performed for two non-equivalent azimuthal directions, verified via LEED to be the directions 0° and 30° as indicated in the inset of Fig. 1.

The final total, positive and negative ion fractions were determined through two independent experiments: i) measurement of the total ion fraction and ii) measurement of positive and negative ion fractions. In the first case, after scattering off the surface, the ions are separated from the neutral particles by a pair of deflection plates placed at the entrance of the drift tube and then detected by three anodes placed behind two microchannel plates (MCP) mounted at the end of the drift tube. In this way, two spectra are obtained: total (ion plus neutrals) and only neutral particles. In the second case, a second set of deflection plates located right before the MCPs allows for discrimination between positive and negative particles, which

are collected by the same anode, each on its own spectrum. The sample-detector distance in our spectrometer is 137 cm. The geometric configuration and the experimental setup are shown in Fig. 1.
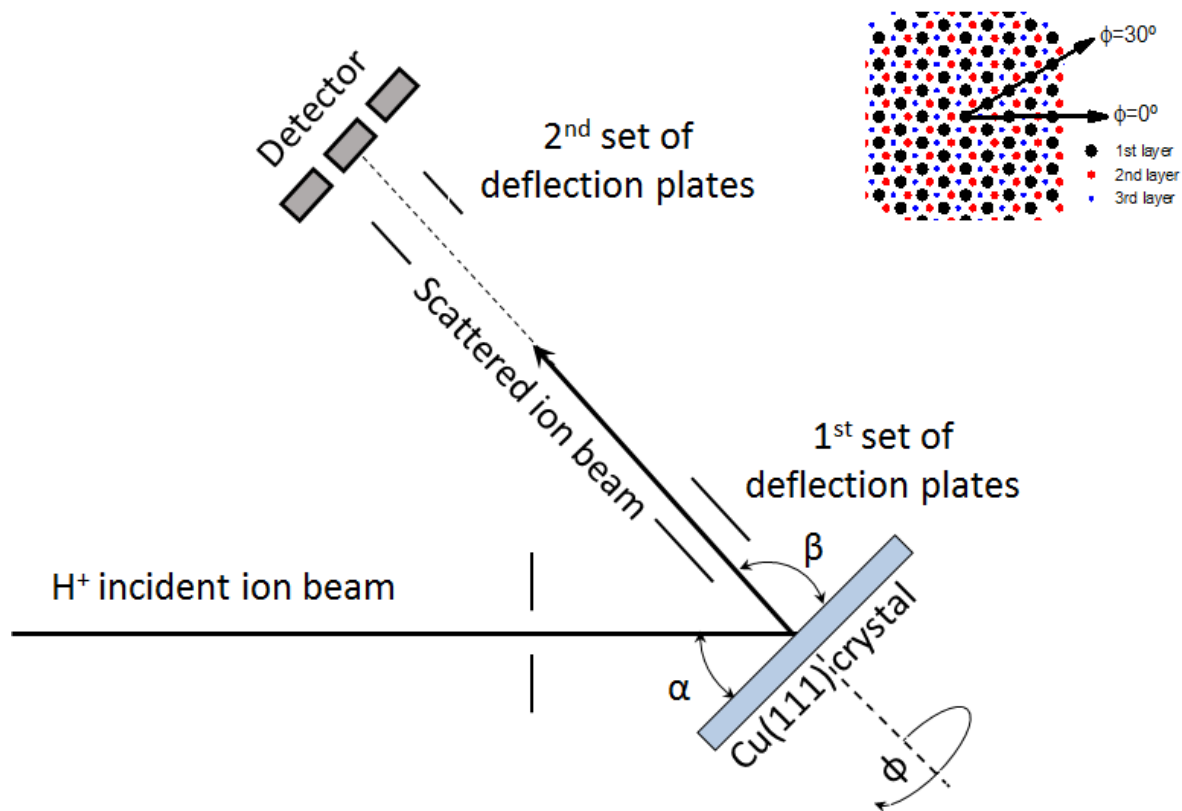

Figure 1: Experimental setup used to obtain the positive, negative and total ion fractions in the TOF-LEIS experiment. The incident (α), exit (β) and azimuthal (φ) angles are detailed. Inset: Top view of the Cu(111) crystalline structure showing the corresponding arrangement of atoms. The azimuthal directions φ=0° and φ=30°, experimentally verified via LEED, are described in this context. Incidence of the ion beam is from left to right as arrows indicate.

The Cu(111) monocrystal target was mounted on a conventional manipulator that allows for reproducible variations of the incident (α), exit (β) and azimuthal (φ) angles (see Fig. 1). The Cu(111) target surface was periodically cleaned by repeating cycles of 3keV Ar^+ small-angle bombardment (20° from the surface) and annealing reconstruction at 550 °C during 5 min. We

made use of Auger spectrometry to verify the cleanliness of the sample and LEED to assess its orientation and order.

Fig. 2 shows the TOF spectra obtained for the two independent experiments described above, at 5keV incident energy of the H^+ projectiles. Total (ions plus neutrals) and neutral particles scattered off the Cu(111) target are depicted in the main body of Fig. 2. The TOF spectra for positive and negative ion fractions are shown in the inset of the same figure. Since we are only interested in electron exchange processes that take place in binary collisions, the experimental ion fractions are obtained integrating a reduced TOF interval around the elastic peak position (indicated as a shadow region in Fig. 2). Particles with larger TOFs might have penetrated to subsurface layers, where multiple collision processes could trigger various charge exchange mechanisms, beyond the theoretical model considered.
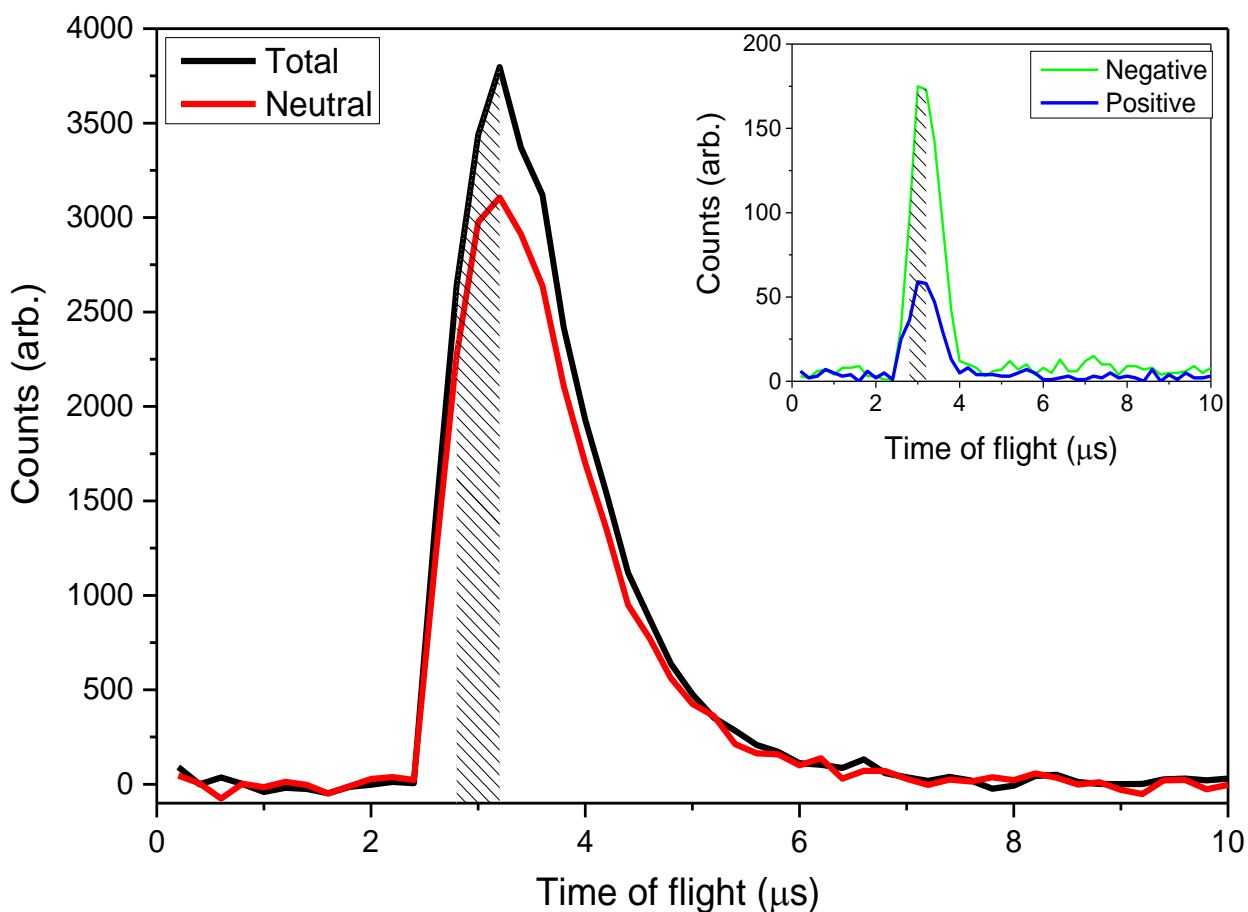

Figure 2: *TOF-LEIS spectra of total and neutral H^+ ions scattered off a Cu(111) surface, with an incoming energy of 5KeV and incident, exit and azimuthal angles of 45º, 90º and 0º, respectively. The corresponding*

negative and positive spectra are shown in the inset. The shadowed area indicates the elastic peak width

considered for the ion fractions calculations.

3. THEORETICAL APPROACH

The Anderson-Newns Hamiltonian,

$$\hat{H} = \sum_{\vec{k},\sigma} \varepsilon_{\vec{k}} \hat{n}_{\vec{k}\sigma} + \sum_{\sigma} \left(\varepsilon_I + U\hat{n}_{a-\sigma} \right) \hat{n}_{a-\sigma} + \sum_{\vec{k},\sigma} \left(V_{\vec{k}a} \hat{c}^+_{\vec{k}\sigma} \hat{c}_{a\sigma} + c.c. \right), \tag{1}$$

provides an adequate framework for studying the resonant charge exchange process occurring due to the interaction of a *s*-valence (as in the case of hydrogen) atom with a metal surface. In eq. (1) the index $\vec{k}$ indicate the solid band state $\psi_{\vec{k}}$ with energy $\varepsilon_{\vec{k}}$; the index *a* refers to the s-valence orbital of the atom with ionization energy ε_I and *U* is the intra-atomic coulomb repulsion in this orbital. The operator $\hat{c}^+_{\alpha\sigma} (\hat{c}_{\alpha\sigma})$ creates (destroys) an electron with spin projection σ in the α-state and $\hat{n}_{\alpha\sigma}$ is the respective occupation number operator. Finally, the coupling term $V_{\vec{k}a}$ takes into account the interaction between the metal band and the atom states.

A successful application of the Anderson-Newns Hamiltonian to the atom-surface interaction strongly depends on a good calculation of the $V_{\vec{k}a}$ term. It has been found [43] that, by expanding the solid states $\psi_{\vec{k}}$ in an atomic basis centered on the atoms of the solid, $\psi_{\vec{k}}(\vec{r}) = \sum_{\alpha,\vec{R}_m} c^{\vec{k}*}_{\alpha,\vec{R}_m} \varphi_\alpha(\vec{r} - \vec{R}_m)$, the $V_{\vec{k}a}$ term can be calculated as:

$$V_{\vec{k}a} = \left\langle \psi_{\vec{k}} \middle| V \middle| \phi_a \right\rangle = \sum_{\alpha,\vec{R}_m} c^{\vec{k}*}_{\alpha m} \left\langle \varphi_\alpha(\vec{r} - \vec{R}_m) \middle| V \middle| \phi_a(\vec{r} - \vec{R}) \right\rangle, \tag{2}$$

where the atom-atom coupling term $V_{\alpha m,a}(\vec{R}) = \left\langle \varphi_\alpha(\vec{r} - \vec{R}_m) \middle| V \middle| \phi_a(\vec{r} - \vec{R}) \right\rangle$ is referred to a symmetrically orthogonalized atomic basis set [44] in the dimer space formed by the projectile atom at the position $\vec{R}$ and the surface atom at $\vec{R}_m$ (both positions are measured with respect to a common origin chosen at the surface scatter atom). The electron-nuclei and electron-electron interactions within a mean field approximation are involved in the calculation model of these atomic coupling integrals [43]. According to eq. (2), the knowledge of the wave functions $\psi_{\vec{k}}(\vec{r})$ is

8

in principle required. But, as we will see later, in our calculation of the charge exchange between the atom and the surface, this information enters through the density matrix of the solid defined as:

$$\rho_{\alpha m, \beta m'}(\varepsilon) = \sum_{\vec{k}} c_{\alpha m}^{\vec{k}*} c_{\beta m'}^{\vec{k}} \delta(\varepsilon - \varepsilon_{\vec{k}}) \qquad (3)$$

Then, on one side we need good atomic basis sets [45,46] to calculate the atom-atom coupling terms (eq. (2)), and, on the other side, an accurate calculation of the density matrix of the solid surface (eq. (3)). This matrix is calculated within the Density Functional Theory (DFT) approach as implemented in the FIREBALL package [47], considering a slab of 6 layers in a 5x5 supercell. This code uses numerical atomic-like orbitals as a basis set, which is adequate for the formalism used in this work. A lot of different atom-surface interacting systems have been described by using this theoretical proposal and in most cases a good agreement with the experimental data has been obtained [9,11,13,32,34-36,48-52].

The ion scattering by a surface is a time dependent process due to the motion of the ion projectile with a finite velocity, $\vec{v}$. For the incoming energies involved, the ion projectile can be considered to move along a classical trajectory with constant velocity, which is well approximated by straight lines given by $\vec{R}(t) = \vec{R}_{tp} + \vec{v}_{in(out)}|t|$, where $\vec{v}_{in(out)}$ is the velocity along the incoming (exit) part of the ion trajectory, $\vec{R}_{tp}$ is the turning point occurring at the closest distance of approach to the surface and $t = 0$ is chosen as the time for which the projectile reaches the turning point.
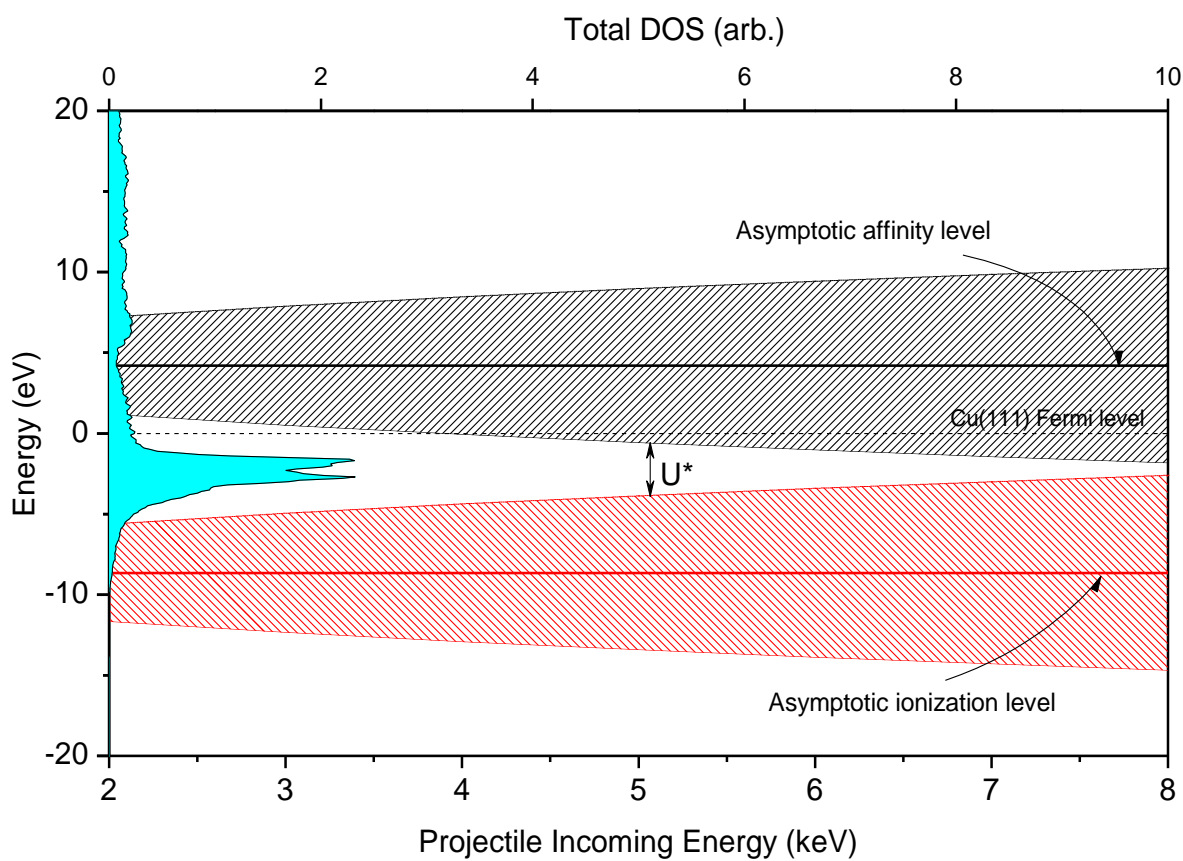
For the case of a hydrogen atom the valence state admits up to two electrons. The probabilities of being negatively (P^-), neutrally (P^0) or positively charged (P^+) are defined as follows:

$$\begin{aligned} P^-(t) &= \langle \hat{n}_{a\uparrow}(t)\hat{n}_{a\downarrow}(t) \rangle \\ P^0(t) &= \langle \hat{n}_{a\uparrow}(t) \rangle + \langle \hat{n}_{a\downarrow}(t) \rangle - 2\langle \hat{n}_{a\uparrow}(t)\hat{n}_{a\downarrow}(t) \rangle \\ P^+(t) &= 1 - P^0(t) - P^-(t) \end{aligned} \qquad (4)$$

9

Therefore, it is enough to calculate the average single $\langle \hat{n}_{a\sigma}(t) \rangle$ and double $\langle \hat{n}_{a\uparrow}(t)\hat{n}_{a\downarrow}(t) \rangle$

occupations to determine the probabilities of the different atomic configurations. To obtain

these quantities we use the following Green-Keldysh [53] functions:

$$G_{aa,\sigma}(t,t') = i\Theta(t'-t)\left\langle \left\{ \hat{c}^{+}_{a\sigma}(t'), \hat{c}_{a\sigma}(t) \right\} \right\rangle$$

$$F_{aa,\sigma}(t,t') = i\left\langle \left[\hat{c}^{+}_{a\sigma}(t'), \hat{c}_{a\sigma}(t) \right] \right\rangle \tag{5}$$

where $[\bullet,\bullet]$ and $\{\bullet,\bullet\}$ are commutator and anticommutator symbols respectively; and $\langle \bullet \rangle$

represents the average over the Heisenberg state Φ_0 that describes the interacting system. The

Green functions (5) are calculated within a second order perturbation treatment of the

correlation parameter U [36,54]. The small U approximation is justified in terms of the uncertainty of

the projectile energy level introduced by the ion velocity, given by $\Delta E_{un} \approx v/2$ in atomic units [36],

which reduces the coulomb repulsion to an effective value U^*. This effect is shown in Fig. 3.

Figure 3: *Asymptotic ionization and affinity one electron energy levels and their inherent velocity uncertainty widths,* ΔE_{un}, *shown as a function of the projectile incoming energy. The effective Coulomb repulsion, U*, is indicated for 5keV incoming energy. The total Cu(111) density of states is also shown.*

4. RESULTS AND DISCUSSION

4.1 Experimental Results

The dependence with the azimuthal angle was assessed by determining the ion fraction for two structurally different crystalline directions, $\varphi=0°$ and $\varphi=30°$ (see Fig. 1). Provided that only the first atomic layer is taken into account, other directions such as $\varphi=60°$ or $\varphi=90°$ are equivalent to $\varphi=0°$ or $\varphi=30°$, respectively. Since LEIS is a technique extremely sensitive to the very first atomic layer, these other directions were disregarded despite the crystalline structure of Cu(111) presents a rotational symmetry of 120°.

Fig. 4 shows the positive, negative and total ions fractions as a function of the incoming energy of the projectile for the two analyzed azimuthal directions and for α/β=45°/90°. For a particular energy, results were obtained after three independent set of experiments. Each experiment involves the measurement of 10 positive, negative, total and neutrals spectra respectively, as described in section 2. Plotted error bars represent the statistical error of this set of measurements.
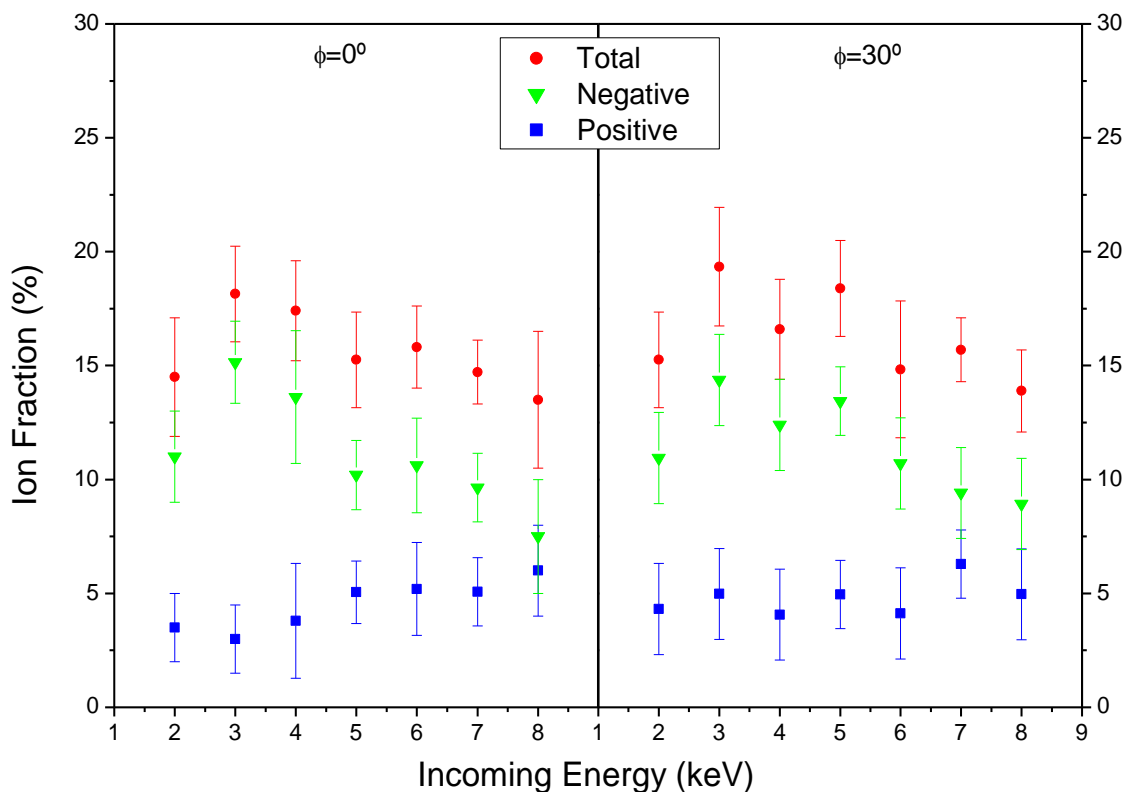
Figure 4: Ion fractions obtained for two different azimuthal directions: $\varphi=0°$ (left) and $\varphi=30°$ (right) and incoming/exit angles of 45°/90°. Results for total (full red circles), negative (full green triangles) and positive (full blue squares) ion fractions are shown as a function of the projectile incoming energy.

To experimentally assess the influence of the incoming and exit angles in the charge transfer process of this system, Fig. 5 compares the ion fractions as a function of the projectile incoming energy obtained for two different incoming/exit angles: 45°/90° and 67.5°/67.5°. The scattering angle is keeping fixed at 135° and the azimuthal direction is $\varphi=0°$.
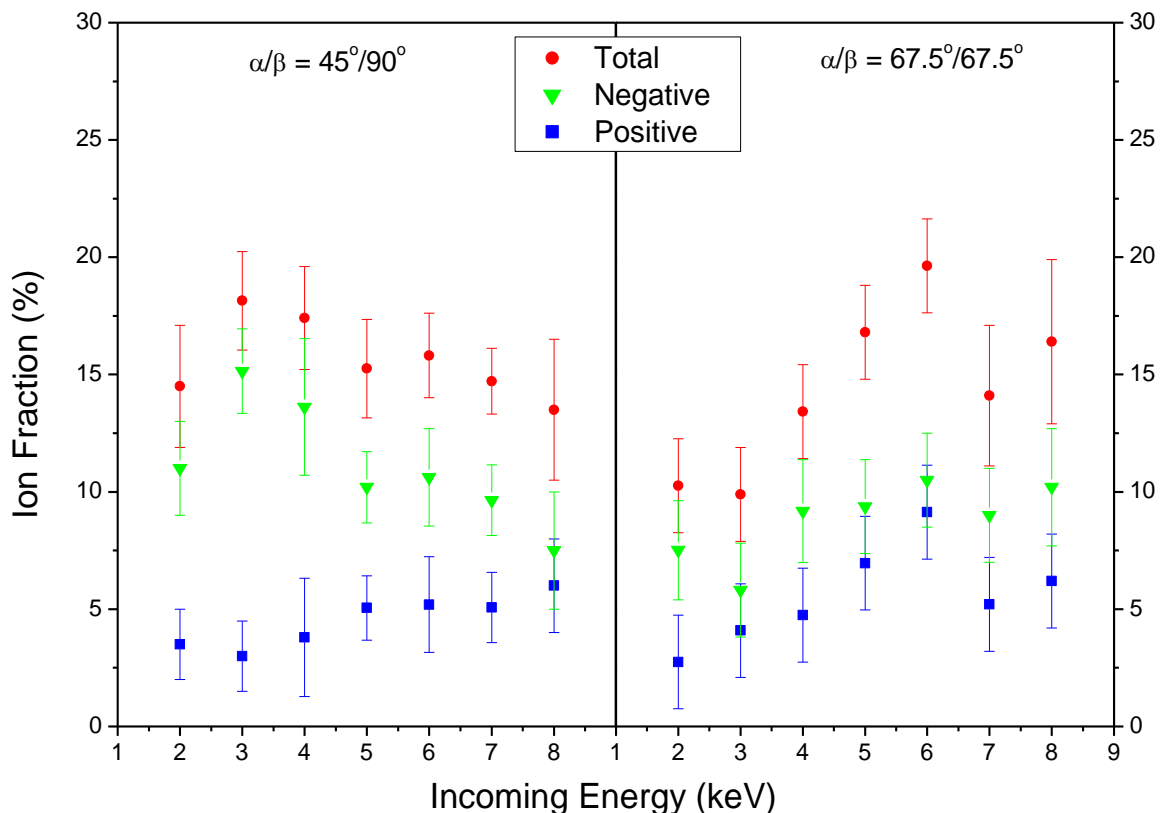
Figure 5: *Ion fractions obtained for two different incoming/exit angles: α/ϐ=45°/90° (left) and α/ϐ=67.5°/67.5° (right). Results for total (full red circles), negative (full green triangles) and positive (full blue squares) ion fractions are shown as a function of the projectile incoming energy. The azimuthal angle is φ=0°.*

Five main features characterize the experimentally obtained results: i) no appreciable differences are observed in the general trend or in ion fractions magnitudes for both azimuthal directions, even when some slight differences (within the experimental error) are observed; ii) a substantial dependence on the incoming/exit angles is found even when the ion fraction magnitudes are not highly altered: dissimilar dependences of the total and negative measured ion fractions with the projectile incoming energy were found for the two incoming/exit angles analyzed ; iii) the negative ion fraction exceeds that of positive ions in the whole energy range studied, regardless the geometry of the experimental setup ; iv) the total ion fraction dependence with the incoming energy is mostly determined by the negative ion fraction dependence; and v) concerning the ion fraction magnitudes, the negative ion fraction formation

ranges from about 8% to 15%, while the positive ion fraction remains lower than 10% in the entire energy span measured. Due to i), from now on, all the experimental results will be shown at $\varphi=0^o$.

The analysis of the ion fraction energy dependence for each scattering geometry indicates that small variations of the ion velocity component parallel to the surface introduce appreciable changes in the charge exchange process. On the contrary, the ion fractions measured in the scattering of protons by a HOPG surface in the same range of incoming energies [36], show very similar trends and magnitudes for two rather different experimental collisional geometries: α/β=45°/90° and 15° /30° (see Fig. 1 of Ref.[36]). The peculiarities of the electronic structure of the Cu(111) surface, such as the projected band-gap in the direction normal to the surface and the presence of a localized surface state, are certainly making the projectile final charge state more sensitive to the ion trajectory.

The negative ion fractions obtained at 2keV incoming energy for α/β=45°/90°, can be contrasted to that shown in Fig. 4 of ref. [31]. Selecting in this figure the negative ion fraction that corresponds to the geometric configuration closest to that of our experiment (α=40°, β=90°), they obtained 8% and we measured around 11%. We think that both results show a reasonable agreement considering the experimental error and the differences in: i) the target used in ref. [31] is a polycrystalline Cu sample, ii) the method to determine the ion fraction (they make use of the whole TOF spectra while we select only the elastic peak) and iii) the slight difference in the geometry between both experimental setups.

4.2 Theoretical Results

The time variation of the Green functions (5) is determined by the self-energy terms which are related to both, the interaction of the atomic orbital with the band states and the electronic repulsion in the projectile atom [36,54]. The self-energy term originated in the atom-solid interaction is given by:

$$\Xi_V^R(t,\tau) = -i\Theta(t-\tau)\sum_{\vec{k}} V_{a\vec{k}}(\vec{R}(t)) V_{\vec{k}a}(\vec{R}(\tau)) e^{-i\varepsilon_{\vec{k}}(t-\tau)} \tag{6}$$

By introducing eq. (2) in eq. (6) and then using the expression (3), we arrive to:

$$\Xi_V^R(t,\tau) = -i\Theta(t-\tau) \sum_{\alpha m, \beta m'} V_{a,\alpha m}(\vec{R}(t)) V_{\beta m',a}(\vec{R}(\tau)) \int d\varepsilon \rho_{\alpha m, \beta m'}(\varepsilon) e^{-i\varepsilon(t-\tau)} \qquad (7)$$

It is clear from expression (7) that the more or less localized nature of the hopping interaction between the projectile and the substrate atoms ($V_{a,\alpha m}$) together with the features of the surface band structure ($\rho_{\alpha m, \beta m'}$), are determinant parameters in the charge transfer process. In the case of a static process where the atom position does not depend on time, the imaginary part of the Fourier transform of eq. (7) gives the Anderson hybridization width:

$$\Gamma(\varepsilon, \vec{R}) = \pi \sum_{\alpha m, \beta m'} V_{a,\alpha m}(\vec{R}) V_{\beta m',a}(\vec{R}) \rho_{\alpha m, \beta m'}(\varepsilon) \qquad (8)$$

Eq. (8) evaluated in either the ionization or the affinity level, provides an estimation of the respective level broadening by the interaction with the band states of the solid surface.

4.2.1   Atom-atom hopping analysis.

The number of surface atoms relevant in the calculation strongly depends on the projectile-target interaction extent and the collisional geometry. In grazing trajectories the projectile ion interacts with more surface atoms than in collisions with high incident and exit angles. As a frontal collision is assumed in our theoretical model, the atom-atom hopping integral $V_{a,\alpha m}(\vec{R})$ will be critical to determine the total number and the particular positions of the Cu(111) atoms that will interact with the projectile.

In Fig. 6 we show the ion-surface distance dependence of the coupling terms $V_{a,\alpha m}(\vec{R})$ between the 1s orbital of the projectile and different valence states of the Cu(111) scatter atom. It is clear from this figure that only 3 states of the Cu surface significantly contribute to the ion-surface interaction: $3d_{z2}$, 4s and $4p_z$ when only the interaction with the scatter atom is considered. This result is a consequence of the projectile-scatter atom frontal collisional geometry assumed.

The extent of the interaction is also clearly determined from fig. 6 to be around 10 a.u.. For longer distances the hopping is nearly zero. Thus, it is expected that only scatter neighbor atoms located within a distance of up to 10 a.u. (~5Å) of the scatter atom might interact with the projectile. The relevant atoms of the Cu(111) crystalline structure, a total of 37 atoms (the scatter plus 36 neighbor atoms), are shown in the inset of Fig.6.
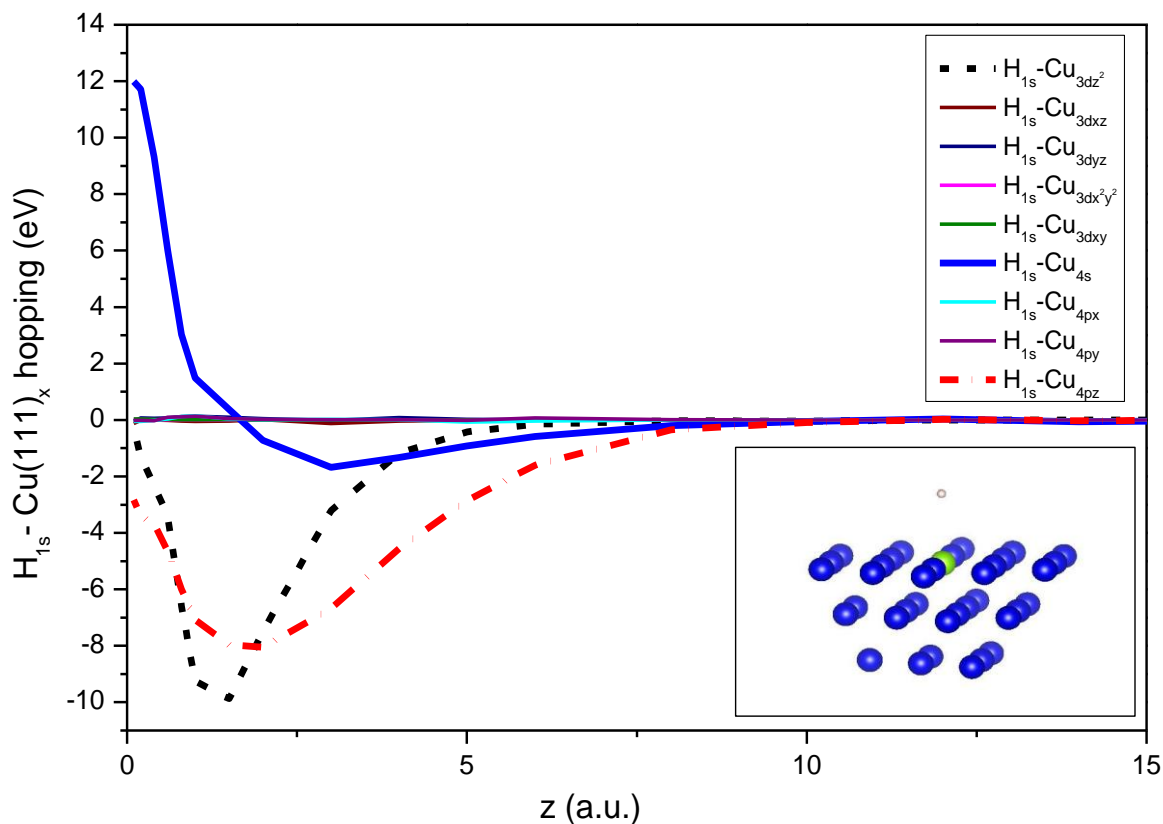
15

Figure 6: *Ion-surface distance (z) dependence of the hopping interaction between the H*(1s) *projectile state and the different Cu valence states of the scatter surface atom. Due to symmetry reasons, only the 3dz², 4s and 4pz Cu states provide significant interactions. The relevant hoppings do not extend over 10a.u.. Inset: scheme of the only relevant surface Cu(111) atoms (blue), considering the hopping extension. The H projectile atom (pink) and the scatter surface atom (green) are distinguished for convenience.*

Taking into consideration the extension of the hopping integrals, a total of 37 atoms (the scatter plus 36 neighbor atoms) will be relevant to the H-Cu charge transfer process during the collision.

4.2.2 Level width analysis.

In Fig. 7, the width of the ionization and affinity levels of hydrogen, $\Gamma(\varepsilon_I, \vec{R})$ and $\Gamma(\varepsilon_I + U, \vec{R})$ respectively, are plotted as a function of the projectile-surface distance when up to first, second, third, fourth and fifth nearest neighbors of the scatter atom are considered. These configurations correspond to 10, 13, 28, 37 and 49 Cu atoms, respectively. The calculations shown in this figure were performed by considering the ion levels only shifted by the image

16

potential for distances to the surface larger than 7 a.u. and the image plane located at 2.091 a.u. [55]
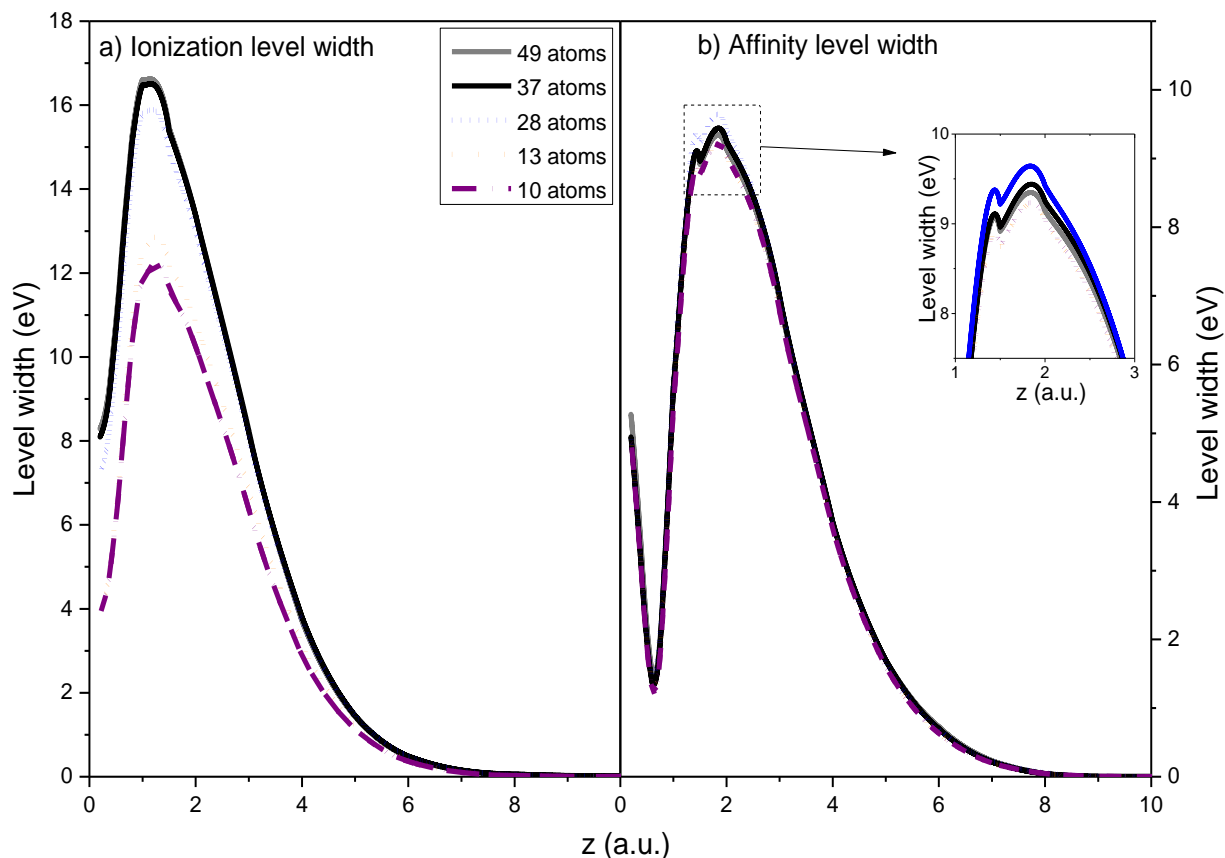

Figure 7: *(a) Ionization and (b) affinity hydrogen level widths as a function of the projectile-surface distance, calculated by considering different number of Cu surface atoms.*

It is clear from Fig. 7 that, as a consequence of the extension of the projectile-surface atom coupling terms $V_{a,\alpha m}(\vec{R})$, the level widths are insignificant for ion-surface distances higher than around 10 a.u. or even lower. In the dynamic problem, this implies that the final charge state of the scattered ion should be already defined around this distance.

The effect of the interference terms due to the Cu (111) band structure details, introduced by the density matrix of the substrate in Eq.(8), leads to a non-monotonous dependence of the affinity level width with the number of substrate atoms involved in the interaction (see the inset in Fig. 7b).

The convergence is more clearly achieved for the affinity level, where a lower number of surface atoms seems to be necessary. For the ionization level, convergence is nearly accomplished when up to fourth nearest neighbors (37 atoms) are included in the target surface. In short, including 37 atoms to describe the Cu(111) target surface should be enough to ensure that the calculated ion fractions will not be altered by adding more surface atoms.

This result should be contrasted with that of Ref. [36] where notably, in the case of a H/HOPG system, only 4 carbon surface atoms are sufficient to adequately describe the dynamic charge transfer problem. The lower number of surface atoms required in the H/HOPG case is a consequence of the greater localization of the electronic distribution of the C atoms compared to that of the Cu atoms. In addition, for a Li/Cu(111) system it was found that 37 surface atoms are needed to be considered [35], the same as in the present H/Cu(111) system. This suggest that the convergence with the number of atoms is mainly determined by the band structure features of the surface and not by the projectile considered.

4.2.3 Band structure analysis.

The band structure obtained and used in our dynamic charge transfer calculation is shown in Fig. 8. We can observe that the L-gap extends from 6.03eV to -1.54 eV (the energies are measured respect to the Fermi level). The surface state falls inside the band gap at an energy equal to -0.44 eV.

The energy position of the surface state is in good agreement with the value -0.38 eV reported by Chulkov et al. [55], while the L-gap width is larger than that calculated also in [55], which extends below the vacuum level from 4.26eV to -0.88 eV.
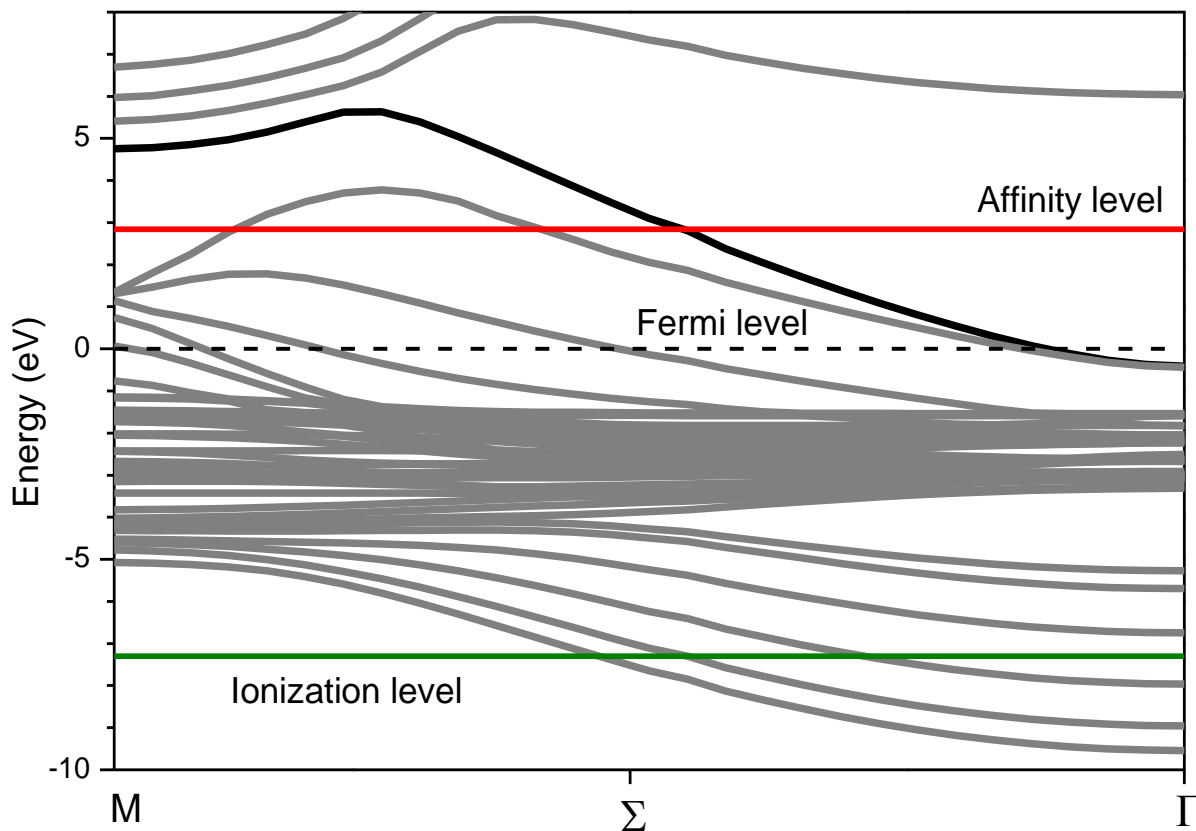
Figure 8*: Projected electronic structure of a Cu(111) surface for selected electron momentum parallel to the surface. The gray lines indicate the quasi-continuum band states and the black solid line corresponds to the surface state. The affinity and ionization hydrogen energy levels are also indicated.*

4.2.4 Ion fraction calculation: details and analysis.

The calculation of the final charge state probabilities P^+ and P^- (eq. (4)) was performed by assuming a trajectory perpendicular to the surface with the incoming (v_{in}) and exit (v_{out}) velocities equal to the perpendicular component of the velocity v in the experimental situation ($v_{in(out)} = v sin\alpha(\beta)$). In the exit trajectory the ion energy is reduced by the corresponding kinematic factor 0.947 of the H-Cu binary collision for a 135° scattering angle. The distance of closest approach was chosen to be 0.2 a.u., according to the interaction energy of the Cu-H dimer. The azimuthal angle considered in all the calculations is $\varphi=0°$.

It was necessary to consider 36 neighbors of the scatter atom to achieve the convergence of the calculated ion fractions (see Eq.(7)), in agreement with the calculation of the ion level widths shown in Fig. 7.

The ionization and affinity levels were shifted, upward and downward respectively, by the image potential $1/4(z - z_{im})$ with $z_{im} = 2.091 a.u.$ [55], for distances z to the surface larger than 7a.u.. The theoretical results do not practically change with the matching distance chosen between 6 and 8 a.u.. If the image potential is disregarded, the same dependence of the ion fractions with the incoming energy is obtained. Nevertheless, the agreement with the experiment was slightly improved when considering the shift by the image potential.

In Fig. 9 we contrast the ion fractions obtained using the small U approximation and the large U approximation described in Ref. [36], for a situation analogous to the specular geometric experimental situation (normal trajectory, with $v_{in} = v_{out} = v \sin 67.5^o$). The energy level positions and the H-Cu interaction summarized by the Anderson hybridization widths, $\Gamma(\varepsilon_I, \vec{R})$ and $\Gamma(\varepsilon_I + U, \vec{R})$, are the same for both calculations. Very important differences between both approximations are found. While the large-U calculation leads to a positive ion fraction notably larger than the negative ion fraction in the whole range of incoming energies, a higher negative yield is obtained in almost the whole range of energies studied when the small-U approach is used (only for 3keV incoming energy, the positive ion fraction is larger). In view of the measurements shown in Fig. 5 and the analysis performed in the theoretical section (see Fig.3), we conclude that the small-U approximation is more adequate to better describe the correlation between the three charge states in the scattering of protons by a Cu(111) surface, in the range of incoming energies between 2 and 8 keV.
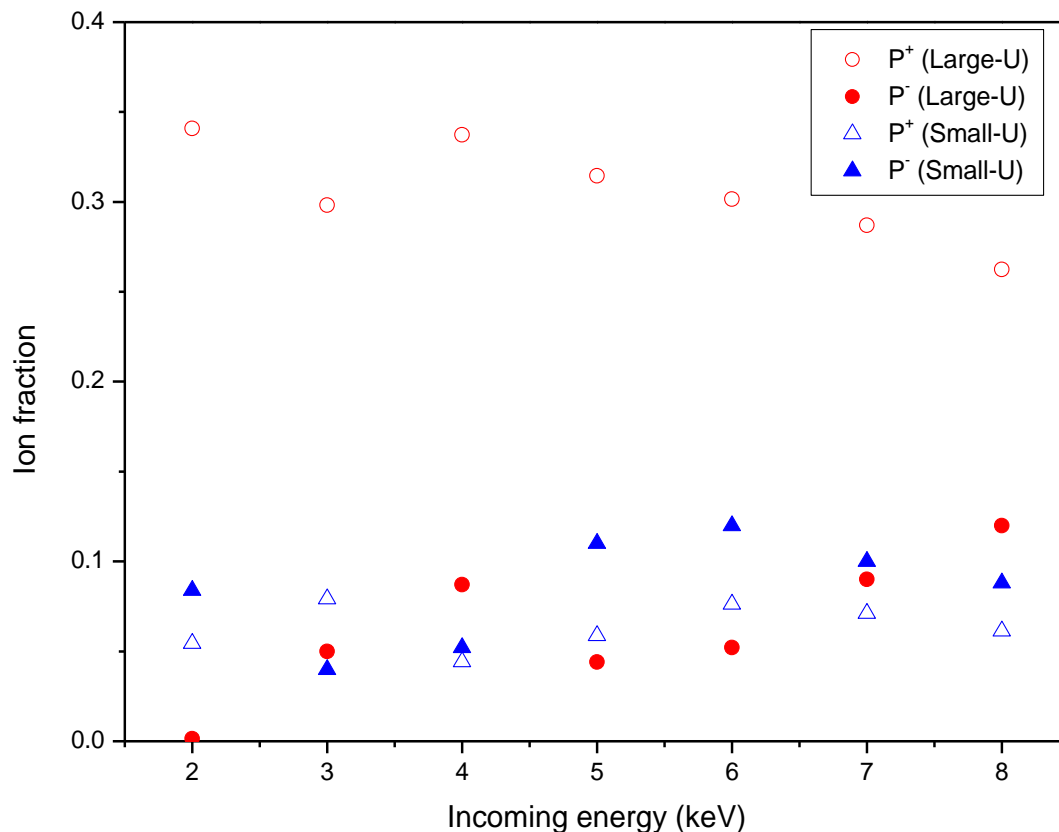
Figure 9: *Positive (empty symbols) and negative (full symbols) ion fractions as a function of the incoming energy, calculated by using the small-U (triangles) and large-U (circles) approximations. A normal trajectory with $v_{in} = v_{out} = v \sin 67.5^o$ is assumed.*

In Figs. 10a and 10b the calculated negative and positive ion fractions (Eq. (4)), respectively, are contrasted for both experimental scattering geometries and two different initial charge states of the projectile hydrogen atom: positive (0,0) and negative (1,1).

We observe that in general the sensitivity to the initial condition becomes more marked as the incoming energy is larger. The slow ion motion leads to a memory loss of the initial charge along the incoming trajectory, as it is clearly observed for the slowest approach to the surface occurring in the 45°/90° scattering geometry.

We can see from figures 10a and 10b, respectively, that both, the survival probabilities of negative and positive incoming ions increase for large kinetic energies of the projectile. This is also an intuitive result since the charge transfer process becomes less possible as the interaction time becomes shorter.

It is necessary to bear in mind that our calculation assumes a normal trajectory for both scattering geometries, meaning that the parallel component of the projectile velocity is always zero. The differences between both scattering geometries in our calculation only arise from the different perpendicular components of the projectile velocity involved in the experimental arrangement. Then, the similar behaviors and magnitudes obtained for both, negative and positive ion fractions, induce to think that the form in which the projectile 'sees' the surface is dominating the energy dependence of the ion fraction.
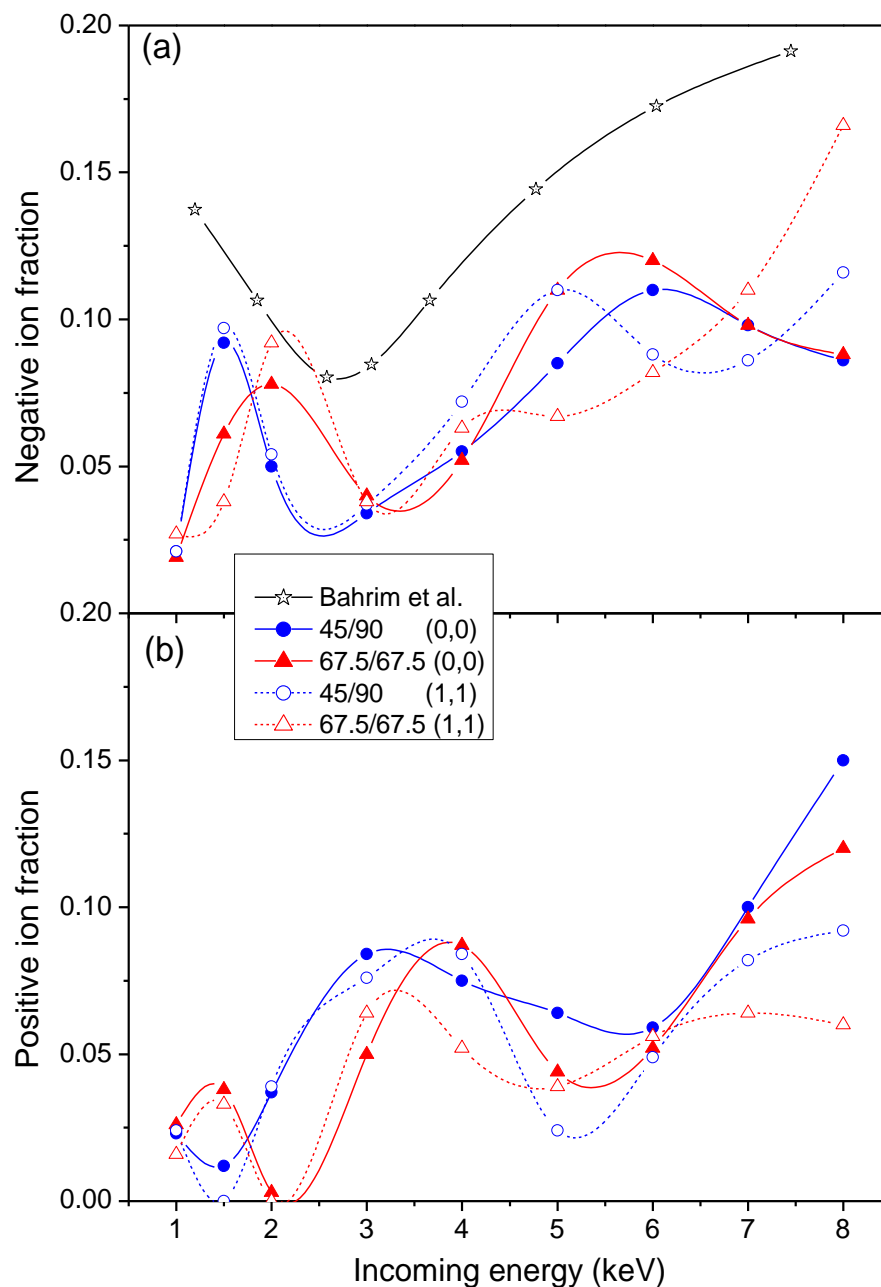
Figure 10: *The calculated negative (a) and positive (b) ion fraction as a function of the incoming projectile energy for the scattering geometries α/β = 45°/90° (circles) and 67.5°/67.5° (triangles). Results are presented for two initial charge states: positive hydrogen (full symbols) and negative hydrogen (empty symbols). Star symbols correspond to the calculation for the 90°/90° geometry performed in Ref.* [31] *assuming a negative initial condition. The lines are only to guide the eyes.*

The positive ion fraction (Fig. 10b) seems to be more sensitive to both, initial charge state and scattering geometry. An important result is the oscillatory behavior with energy of both ion fractions, evidencing the charge exchange between the localized surface state of the Cu(111) surface and the affinity ion level. The oscillations are more pronounced as the energy is lower and the presence of the L-gap becomes more visible. At low projectile velocities, the affinity level immersed in the L-gap (Fig.8) combined with the energy uncertainty inherent to the projectile velocity (Fig. 4) make negligible the contribution of the continuous band states in the charge exchange process. The valence band of the Cu(111) begins to contribute to the negative ion formation at larger energies when, within the energy uncertainty, the affinity level overlaps with this band. On the other side, the interaction time begins to become shorter, reducing the charge transfer probability. Then, we can understand the increase of the negative ion fraction for energies larger than 4keV, followed by a decrease at the largest analyzed energy values of 7 and 8keV.

For comparison, in Fig. 10a we show the negative ion fraction calculated in Ref. [31] by using the wave packet propagation technique (WPPT), for an ion movement perpendicular to the surface and assuming an initial negative charge state for the hydrogen projectile (see Fig. 3 in Ref. [31]). They also used a turning point between 0.1 and 0.2a.u., even when the additive electron-projectile core and electron-surface potentials used in the WPPT is not valid at small ion-surface distances [27]. In this calculation the time-evolution of the hydrogen negative ion moving normal to the surface is reduced to the electron loss of a unique electron in the potential formed by the surface and the atom. The electron-Cu(111) surface potential [55] reproduces key features of the bulk and surface electronic structure, such as the width and position of the band gap and the energies of the surface state and first image state at the Γ point. At large distances from the surface this potential behaves as an image-like Coulomb potential.

Our calculation is based on the Anderson model with an ab-initio calculation of the Hamiltonian terms (Eq. (2)) which requires the electronic structure of the Cu(111) surface (Fig. 8) for calculating the density matrix and the atom-atom hopping terms provided by the bond-pair model [43]. Then, we are properly taking into account the L-gap and the localized surface state (Fig. 8), but we are not considering the image state. The image state, contrary to what occurs with the surface state, is located at distances far from the surface, where the interaction of a fast projectile with the surface is almost negligible. Then, we do not expect that the image state has an important incidence in the charge transfer process at the energy range analyzed in this work. In addition, our model contemplates the three possible charge states of hydrogen within a time-dependent quantum process in which the electronic repulsion in the localized projectile state is considered within a second order of perturbation. The correct initial condition of the experiment (proton as projectile) is assumed and electron loss and capture processes are able to occur along the ion trajectory.

Bahrim et al. [31], by using the wave packet propagation method, found for large energies (>4keV) an energy dependence of the negative ion fraction that reproduces the one for a jellium-like surface, and a weak oscillatory behavior for low energies, between 0.1 and 4keV. The authors state that for large velocities the projectile has not enough time to see the peculiar details of the electronic structure of the Cu(111) surface and, therefore, the Coulomb image potential contribution to the electron-surface potential mainly control the charge transfer process. However, for low velocities, the presence of the L-gap blocks the electron transfer to the surface in the normal direction and induces an increase of the survival probability of the negative ions [27,56,57].

Our calculation (Fig. 10a, 45°/90° with a negative initial charge) leads to a similar behavior to that found in Ref. [31] between 2 and 4keV, but the non-monotonous behavior found for energies larger than 4keV is suggesting a charge exchange with the narrow d-band of Cu(111). For energy values below 2keV, it is found a marked oscillation characteristic of the charge exchange between localized states, indicating the interaction of the surface state with the affinity level, both inside the L-gap.

The positive ion fraction (Fig. 10b), calculated within a correlated way with the other two possible charge states of hydrogen, also shows an oscillatory behavior with the incoming energy which is quite complementary of the oscillatory behavior of the negative ion fraction (Fig. 10a).

4.2.5 Comparison between theoretical and experimental results.

In Fig. 11 (left panels) we compare the calculated and measured negative ion fractions for both experimental scattering geometries. Considering the whole energy span studied and despite our calculations show oscillations that can barely be appreciated in the experimental results, our theoretical results reproduce more adequately the experimental data for the specular experimental scattering geometry (67.5°/67.5°).
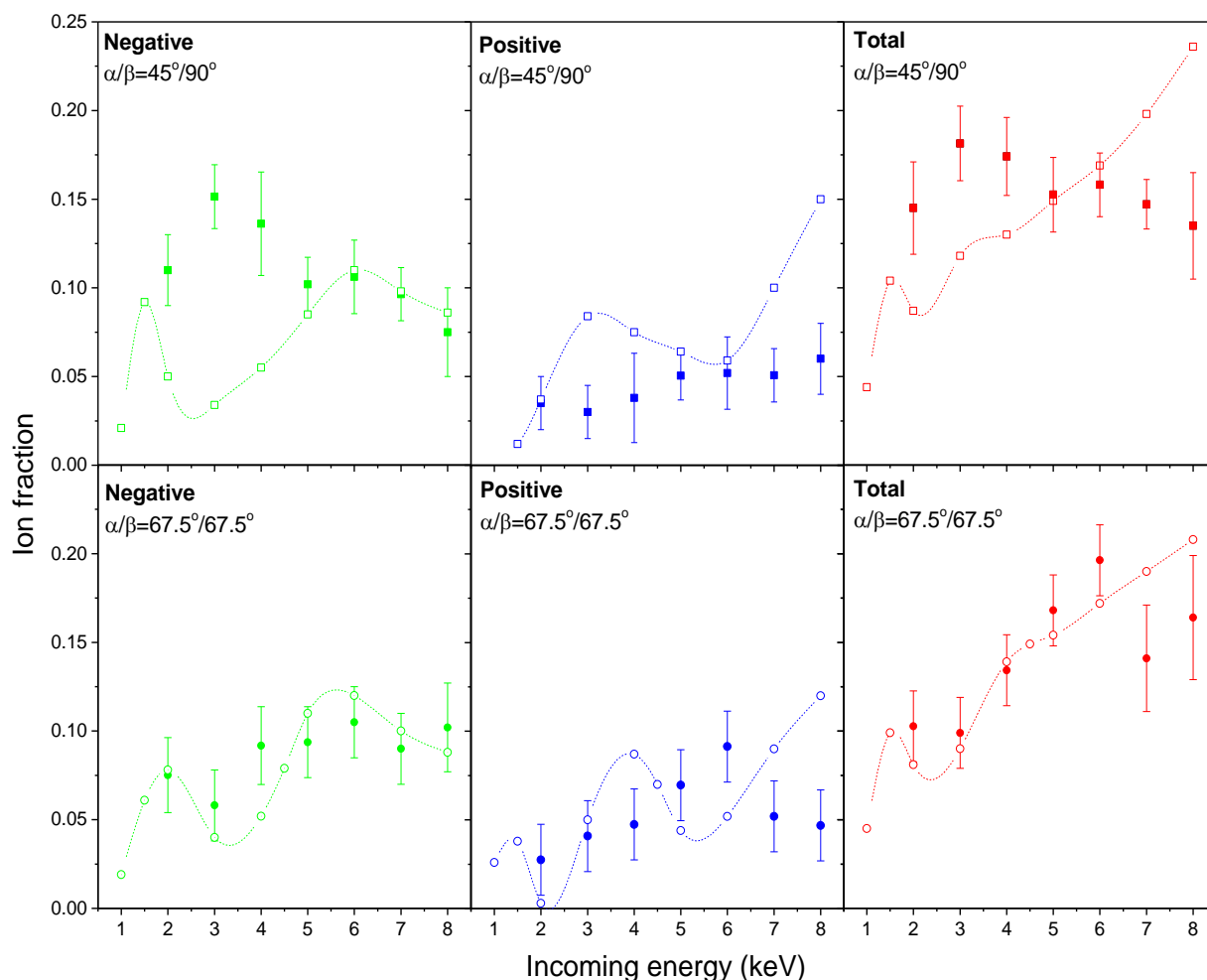

Figure 11: Experimental (full symbols) and theoretical results (empty symbols) are contrasted for negative (left), positive (center) and total (right) ion fractions. Results are shown as a function of the incoming

energy for the two scattering geometries analyzed: 45°/90° (top panels) and 67.5°/67.5° (bottom panels). The lines are only to guide the eyes.

For the $45^0/90^0$ experimental geometry the calculation provides a good description of the experimental negative ion fractions only at large energy values ($\geq$ 5keV). From the comparison between results obtained for both experimental geometries we can infer that, for large kinetic energies, the L-gap and the localized surface state are less relevant than the continuous band states for the charge exchange problem analyzed. Then, at these high energies, the different parallel velocity components for both experimental scattering geometries have a minor effect on the negative ion formation. Similar theoretical results are obtained for both, 45°/90° and 67.5°/67.5°, by assuming a perpendicular trajectory with different incoming/exit velocities in both cases. Then, a comparative analysis of the experimental and theoretical results indicates that the form in which the projectile is seeing the Cu(111) surface is the dominant factor in the charge exchange process.

Unarguably, the experimental positive ion fractions are not precisely described by our model. Oscillations in antiphase observed in the calculated positive ion fractions cannot be directly associated to the Cu(111) surface state. However, as the three charge state channels are correlated in our calculations, these oscillations could be indirectly linked to the surface state, through the negative ion formation. For both scattering geometries, the calculated values overestimate the experimental results for the largest energies (7 and 8keV). The theoretical results show an increase in the positive ion survival for large energies, as expected when other possible neutralization channels are disregarded. In the case of protons colliding with a Cu(111) surface, the neutralization to the hydrogen ground state is not very efficient since the energy position of the 1s level is close to the bottom of the valence band of the Cu surface. Thus, the neutralization to the excited states 2s and 2p may be feasible as well as the formation of excited negative configurations with active energy levels below the vacuum level, as indicated in figure 12. The possibility of neutralization to the excited states is expected to be more important for large kinetic energies of the projectile, and this will finally lead to a decaying positive ion fraction. The inclusion of these many charge configurations implies very complex calculations that are currently beyond our possibilities.
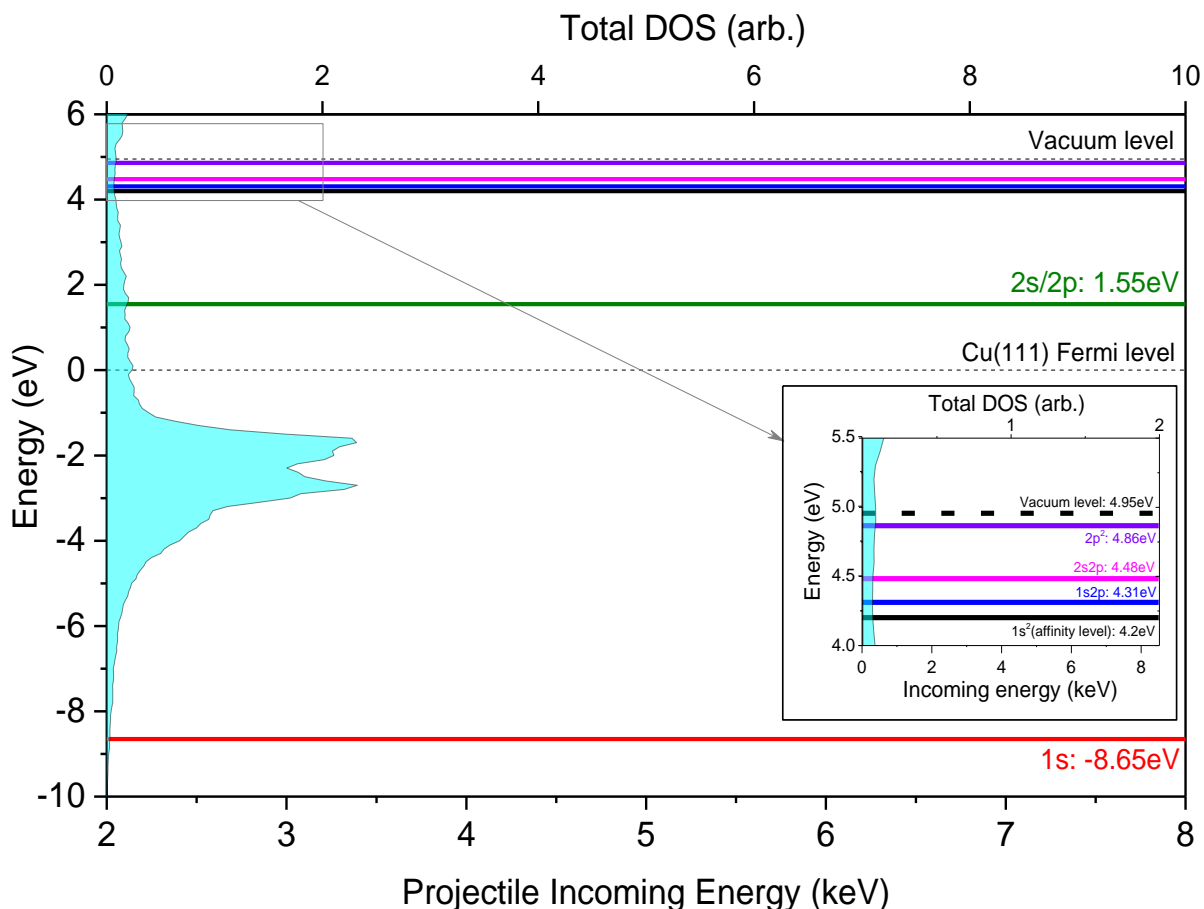
Figure 12: *One electron energy levels that account for neutralization to the ground state (red line, 1s), neutralization to excited states 2s or 2p (olive, 2s/2p), formation of negative 1s² configuration (black, affinity level), formation of negative 1s2p configuration (blue), formation of negative 2s2p configuration (magenta), formation of negative 2p² configuration (violet). The vacuum level, Cu(111) Fermi level and the Cu(111) total DOS are also plotted. Energy level values are extracted from Refs.[58-60]. For the sake of clarity, the region limited by the grey rectangle is zoomed in (inset) and the levels energy values indicated.*

The calculated total ion fraction behavior with energy is inverted with respect to the experimental result for the 45°/90° scattering geometry, while a very good description of the measured total ion fraction is obtained for the specular arrangement up to 6keV (see Fig. 11, right panels).

In summary:

1) The calculated ion fractions, that assume always a normal ion trajectory but different incoming and exit velocities for the two analyzed scattering geometries, lead to very similar results in both, 45°/90° and 67.5°/67.5° scattering geometries.

2) The experimental results show that the energy dependence of the ion fraction changes appreciably with small variations of the scattering geometry.

3) Our calculation reproduces satisfactorily the experimental results for the specular collision geometry.

From 1), 2) and 3) we infer that the characteristics of the Cu(111) surface make the energy dependence of the charge exchange process very sensitive to small changes in the ion trajectory. Since our theoretical results reproduce more satisfactorily the 67.5°/67.5° experimental geometry (with an entrance angle closer to that assumed in our model) we conclude that the incoming angle is playing a major role in the charge exchange between H ions and a Cu(111) surface.

5.   CONCLUSIONS.

We measured the total, positive and negative ion fractions of H^+ ions scattered by a monocrystalline Cu(111) surface. Measurements are presented as a function of the incoming energy of the projectile (from 2-8keV) for a fixed backscattering angle of 135°, two incoming/exit angles and two different azimuthal orientations of the target surface. In order to explain the experimental data we applied a first principles quantum-mechanical formalism based on the Anderson Hamiltonian and the bond-pair model to account for the interaction between projectile and surface atoms. Our model is capable of including electronic correlation effects in the localized projectile state and in this form, takes into account the different charge states of hydrogen. This is crucial in the light of the measured negative and positive ion fractions.

Experimentally, we determined that the ion fractions do not depend on the azimuthal orientation of the Cu(111) surface, but they are quite sensitive to small variations in the incoming/exit angles combination. The total ion fraction varies from 10% to 20%, and a preponderance of negative ions is always measured, irrespective of the scattering geometry. Positive ions, for the first time shown and discussed in this system, vary from 2% to 10% and present a slighter dependence with the incoming energy than that observed for the negative ion

fractions. Strong differences are found on the ion fractions dependence with the incoming energy for both analyzed scattering geometries 45°/90° and 67.5°/67.5°, even when the ion fraction magnitudes do not significantly change when the scattering geometry is altered.

On the theoretical side, the analysis of the interaction hopping of H-Cu atoms allows us to conclude that the whole charge transfer process is accomplished at ion-surface distances lower than 10a.u. The same analysis, added to the ionization and affinity level widths dependence on the number of surface atoms considered, led us to the conclusion that only 37 surface atoms (up to fourth nearest neighbors) are needed to be included in our calculation in order to ensure convergence.

The ion fraction calculation is performed by assuming a trajectory perpendicular to the surface with velocities corresponding to the normal component of the projectile velocities in the experiment. The ion fractions obtained for the 67.5°/67.5° scattering geometry is clearly better described in magnitude and energy dependence by our theoretical model. The incoming angle for the 67.5°/67.5° scattering geometry is the closest to that assumed in the theoretical model. Therefore, the disagreement between the theoretical description and the experimental data for the 45°/90° experimental set-up indicates an important role of the incoming trajectory (or parallel velocity component) in the charge exchange between hydrogen ions and a Cu(111) surface. As expected, this effect becomes more important for lower incoming energies. By comparing with the case of protons colliding with a HOPG surface [36], where the ion fractions practically do not change under similar variations of the scattering geometry, we can conclude that the surface state inside the L-gap, a distinctive feature of the Cu(111) surface, is central to the dynamic charge transfer problem analyzed.

In addition, the disagreement between the measured and calculated energy dependences of the positive ion fraction suggests that the neutralization to excited states may be contributing to the charge exchange process between hydrogen and Cu(111).

REFERENCES

(1)   Brongersma, H. H.; Draxler, M.; de Ridder, M.; Bauer, P. Surface Composition Analysis by Low-Energy Ion Scattering *Surface Science Reports* **2007**, *62*, 63-109.

(2)   Wang, N. P.; García, E. A.; Monreal, R.; Flores, F.; Goldberg, E. C.; Brongersma, H. H.; Bauer, P. Low-Energy Ion Neutralization at Surfaces: Resonant and Auger Processes *Physical Review A* **2001**, *64*, 012901.

(3)   Goswami, R. Influence of Plasma Surface Interactions on Tokamak Startup *Physics of Plasmas* **2013**, *20*, 082516.

(4)   Tokar, M. Z.; Kelly, F. A. The Role of Plasma–Wall Interactions in Thermal Instabilities at the Tokamak Edge *Physics of Plasmas* **2003**, *10*, 4378-4386.

(5)   Kroes, G.-J.; Pavanello, M.; Blanco-Rey, M.; Alducin, M.; Auerbach, D. J. Ab Initio Molecular Dynamics Calculations on Scattering of Hyperthermal H Atoms from Cu(111) and Au(111) *The Journal of Chemical Physics* **2014**, *141*, 054705.

(6)   Lienemann, J.; Blauth, D.; Wethekam, S.; Busch, M.; Winter, H.; Wurz, P.; Fuselier, S. A.; Hertzberg, E. Negative Ion Formation During Scattering of Fast Ions from Diamond-Like Carbon Surfaces *Nuclear Instruments and Methods in Physics Research Section B: Beam Interactions with Materials and Atoms* **2011**, *269*, 915-918.

(7)   Bommel, P. J. M. v.; Geerlings, J. J. C.; Wunnik, J. N. M. v.; Massmann, P.; Granneman, E. H. A.; Los, J. Formation of H− by Scattering H+ on a Cesiated Polycrystalline Tungsten Surface *Journal of Applied Physics* **1983**, *54*, 5676-5684.

(8)   Chalker, P. R. Photochemical Atomic Layer Deposition and Etching *Surface and Coatings Technology* **2016**, *291*, 258-263.

(9)   Bonetto, F.; Gonzalez, C.; Goldberg, E. C. Signals of Strong Electronic Correlation in Ion Scattering Processes *Physical Review B* **2016**, *93*, 195439.

(10)   Gao, L.; Zhu, Y.; Shi, Y.; Liu, P.; Xiao, Y.; Li, G.; Liu, Y.; Esaulov, V. A.; Chen, X.; Chen, L.; Guo, Y. Dynamical Resonant Neutralization of Low-Energy N^+ Ions Scattered from Au(111), Pd(111), Cu(111), and Cu(110) Surfaces *Physical Review A* **2017**, *96*, 052705.

(11)   Iglesias-García, A.; González, C.; Goldberg, E. C. Theoretical Study of the Charge Transfer and Electron Emission in the Scattering of He^+ by an AlF_3 Surface *Physical Review B* **2017**, *96*, 075428.

(12)   Riccardi, P.; Sindona, A.; Dukes, C. A. Local Charge Exchange of He+ Ions at Aluminum Surfaces *Physics Letters A* **2017**, *381*, 1174-1176.

(13)   Tacca, M. S.; Bonetto, F.; Goldberg, E. C. Electronic Correlation Effects on the Neutralization of Ga^+ Scattered by a Gold Surface *Physical Review B* **2017**, *96*, 075424.

(14)   Xiong, F.; Gao, L.; Liu, Y.; Lu, J.; Liu, P.; Qiu, S.; Qiu, X.; Guo, Y.; Chen, X.; Chen, L. Dynamical Resonant Charge Transfer of Fast C−, O−, F− Ions and Water Covered Si(111) Surface *Vacuum* **2017**, *137*, 23-30.

(15)   Bahrim, B.; Stafford, J.; Makarenko, B. Charge Transfer During H/H− Collisions with Cu(100) and Cu(111) Surfaces *Surface and Interface Analysis* **2018**, *50*, 212-219.

(16)   Gao, L.; Zhu, Y.; Shi, Y.; Liu, P.; Xiao, Y.; Ren, F.; Chen, L.; Guo, Y.; Chen, X. Role of Projectile Energy and Surface Work Function on Charge Transfer of Negative Ions Grazing Scattering on Dissociated H2o-Covered Cu(110) *Applied Surface Science* **2018**, *428*, 1082-1088.

(17)   Von Gemmingen, U.; Sizmann, R. Charge States of Slow Hydrogen Ions Reflected at Single Crystal Surfaces *Surface Science* **1982**, *114*, 445-458.

(18)   Van Wunnik, J. N. M.; Geerlings, J. J. C.; Granneman, E. H. A.; Los, J. The Scattering of Hydrogen from a Cesiated Tungsten Surface *Surface Science* **1983**, *131*, 17-33.

30

(19)   Geerlings, J. J. C.; Van Amersfoort, P. W.; Kwakman, L. F. T.; Granneman, E. H. A.; Los, J.; Gauyacq, J. P. H− Formation in Proton-Metal Collisions *Surface Science* **1985**, *157*, 151-161.

(20)   van Os, C. F. A.; Leguijt, C.; Kleyn, A. W.; Los, J. In *Fusion Technology 1988*; Van Ingen, A. M., Nijsen-Vis, A., Klippel, H. T., Eds.; Elsevier: Oxford, 1989, p 598-603.

(21)   Zimny, R.; Nienhaus, H.; Winter, H. Mgo and H− Formation after Grazing Ion-Surface Scattering *Nuclear Instruments and Methods in Physics Research Section B: Beam Interactions with Materials and Atoms* **1990**, *48*, 361-366.

(22)   Wyputta, F.; Zimny, R.; Winter, H. H− Formation in Grazing Collisions of Fast Protons with an Al(111) Surface *Nuclear Instruments and Methods in Physics Research Section B: Beam Interactions with Materials and Atoms* **1991**, *58*, 379-383.

(23)   Borisov, A. G.; Teillet-Billy, D.; Gauyacq, J. P. Dynamical Resonant Electron Capture in Atom Surface Collisions: H⁻ Formation in H - Al(111) Collisions *Physical Review Letters* **1992**, *68*, 2842-2845.

(24)   Kurnaev, V. A.; Koborov, N. N.; Zhabrev, G. I.; Zabeida, O. V. Charge Fractions in a Hydrogen Beam Reflected from Targets with Different Electron Density *Nuclear Instruments and Methods in Physics Research Section B: Beam Interactions with Materials and Atoms* **1993**, *78*, 63-67.

(25)   Maazouz, M.; Borisov, A. G.; Esaulov, V. A.; Gauyacq, J. P.; Guillemot, L.; Lacombe, S.; Teillet-Billy, D. Effect of Metal Band Characteristics on Resonant Electron Capture: H⁻ Formation in the Scattering of Hydrogen Ions on Mg, Al, and Ag Surfaces *Physical Review B* **1997**, *55*, 13869-13877.

(26)   Auth, C.; Winter, H.; Borisov, A. G.; Bahrim, B.; Teillet-Billy, D.; Gauyacq, J. P. O⁻ Formation in Grazing Scattering from an Al(111) Surface *Physical Review B* **1998**, *57*, 12579-12587.

(27)   Borisov, A. G.; Kazansky, A. K.; Gauyacq, J. P. Resonant Charge Transfer in Ion-Metal Surface Collisions: Effect of a Projected Band Gap in the H⁻−Cu(111) System. *Physical Review B* **1999**, *59*, 10935-10949.

(28)   Winter, H. Collisions of Atoms and Ions with Surfaces under Grazing Incidence *Physics Reports* **2002**, *367*, 387-582.

(29)   Bahrim, B.; Makarenko, B.; Rabalais, J. W. Mechanism of Negative Ion Formation in Low Velocity Collisions at Surfaces *Surface Science* **2003**, *542*, 161-166.

(30)   Chakraborty, H.; Niederhausen, T.; Thumm, U. Resonant Neutralization of H⁻ near Cu Surfaces: Effects of the Surface Symmetry and Ion Trajectory *Physical Review A* **2004**, *70*, 052903.

(31)   Bahrim, B.; Makarenko, B.; Rabalais, J. W. Band Gap Effect on H− Ion Survival near Cu Surfaces *Surface Science* **2005**, *594*, 62-69.

(32)   Bonetto, F.; Romero, M. A.; García, E. A.; Vidal, R. A.; Ferrón, J.; Goldberg, E. C. Large Neutral Fractions in Collisions of Li⁺ with a Highly Oriented Pyrolytic Graphite Surface: Resonant and Auger Mechanisms *Physical Review B* **2008**, *78*, 075422.

(33)   Bahrim, B.; Yu, S.; Makarenko, B.; Rabalais, J. W. Electron Dynamics in H−/Na/Cu(111) Collisions *Surface Science* **2009**, *603*, 703-708.

(34)   Vidal, R. A.; Bonetto, F.; Ferrón, J.; Romero, M. A.; García, E. A.; Goldberg, E. C. Electron Capture and Loss in the Scattering of H+ from Hopg Graphite *Surface Science* **2011**, *605*, 18-23.

(35)   Bonetto, F. J.; García, E. A.; González, C.; Goldberg, E. C. Image Potential State Influence on Charge Exchange in Li+−Metal Surface Collisions *The Journal of Physical Chemistry C* **2014**, *118*, 8359-8368.

(36)   Bonetto, F. J.; Romero, M. A.; Iglesias-García, A.; Vidal, R. A.; Goldberg, E. C. Time−Energy Uncertainty and Electronic Correlation in H+−Graphite Collisions *The Journal of Physical Chemistry C* **2015**, *119*, 3124-3131.

(37)   Yu, S.; Bahrim, B.; Makarenko, B.; Rabalais, J. W. H− Survival Probability During Collisions with Na/Cu(111) *Surface Science* **2015**, *636*, 13-18.

(38)   Dudnikov, V.; Dudnikov, A. Positronium Negative Ions for Monitoring Work Functions of Surface Plasma Source *AIP Conference Proceedings* **2017**, *1869*, 020007.

(39)   Hecht, T.; Winter, H.; Borisov, A. G.; Gauyacq, J. P.; Kazansky, A. K. Role of the 2d Surface State Continuum and Projected Band Gap in Charge Transfer in Front of a Cu(111) Surface *Physical Review Letters* **2000**, *84*, 2517-2520.

(40)   Rutigliano, M.; Palma, A.; Sanna, N. Hydrogen Scattering from a Cesiated Surface Model *Surface Science* **2017**, *664*, 194-200.

(41)   Bauer, P. In *Surface and Thin Film Analysis: A Compendium of Principles, Instrumentation, and Applications.*; Friedbacher, P. a. B., H., Ed.; John Wiley & Sons.: 2011.

(42)   Grizzi, O.; Shi, M.; Bu, H.; Rabalais, J. W. Time-of-Flight Scattering and Recoiling Spectrometer (Tof-Sars) for Surface Analysis *Review of Scientific Instruments* **1990**, *61*, 740-752.

(43)   Bolcatto, P. G.; Goldberg, E. C.; Passeggi, M. C. G. Interaction between Atoms and Surfaces: A Bond-Pair Description Based on an Extended Anderson Model *Physical Review B* **1998**, *58*, 5007-5021.

(44)   Löwdin, P. O. On the Non-Orthogonality Problem Connected with the Use of Atomic Wave Functions in the Theory of Molecules and Crystals *The Journal of Chemical Physics* **1950**, *18*, 365-375.

(45)   Huzinaga, S. Gaussian-Type Functions for Polyatomic Systems. I *The Journal of Chemical Physics* **1965**, *42*, 1293-1302.

(46)   Huzinaga, S.; Andzelm, J.; Klobukowsky, M.; Radzio-Andzelm, E.; Sakai, Y.; Tatewaki, H. *Gaussian Basis Sets for Molecular Calculations*; Elsevier: Amsterdam, The Netherlands, 1984.

(47)   Lewis, J. P.; Jelínek, P.; Ortega, J.; Demkov, A. A.; Trabada, D. G.; Haycock, B.; Wang, H.; Adams, G.; Tomfohr, J. K.; Abad, E.; Wang, H.; Drabold, D. A. Advances and Applications in the Fireball Ab Initio Tight-Binding Molecular-Dynamics Formalism *physica status solidi (b)* **2011**, *248*, 1989-2007.

(48)   García, E. A.; Pascual, C. G.; Bolcatto, P. G.; Passeggi, M. C. G.; Goldberg, E. C. Ion Fractions in the Scattering of Hydrogen on Different Reconstructed Silicon Surfaces *Surface Science* **2006**, *600*, 2195-2206.

(49)   Luna, N. B.; Bonetto, F. J.; Vidal, R. A.; Goldberg, E. C.; Ferrón, J. Low Energy Ion Scattering in He/Hopg System *Journal of Molecular Catalysis A: Chemical* **2008**, *281*, 237-240.

(50)   Romero, M. A.; Iglesias-García, A.; Goldberg, E. C. Localized Description of Band Structure Effects on Li Atom Interaction with Graphene *Physical Review B* **2011**, *83*, 125411.

(51)   Meyer, C.; Bonetto, F.; Vidal, R.; García, E. A.; Gonzalez, C.; Ferrón, J.; Goldberg, E. C. Understanding the High Neutralization Yields in Collisions of Kev Li+ Ions with Copper Surfaces *Physical Review A* **2012**, *86*, 032901.

(52)   Iglesias-García, A.; Bonetto, F.; Vidal, R.; Ferrón, J.; Goldberg, E. C. Ion Neutralization and High-Energy Electron Emission in He+ Scattering by a Highly Oriented Pyrolitic Graphite Surface *Physical Review A* **2014**, *89*, 042702.

(53)   Keldysh, L. V. Diagram Technique for Nonequilibrium Processes *J. Exp. Theor. Phys.* **1965**, *20*, 1018-1026.

(54)   Goldberg, E. C.; Passeggi, M. C. G. Correlation Effects in Dynamical Charge-Transfer Processes *Journal of Physics: Condensed Matter* **1993**, *5*, A259.

(55)   Chulkov, E. V.; Silkin, V. M.; Echenique, P. M. Image Potential States on Metal Surfaces: Binding Energies and Wave Functions *Surface Science* **1999**, *437*, 330-352.

(56)   Desjonquères, M. C.; Spanjaard, D. *Concepts in Surface Physics*; Springer-Verlag: Berlin, 1993; Vol. 30.

(57)   Chulkov, E. V.; Silkin, V. M.; Echenique, P. M. Image Potential States on Lithium, Copper and Silver Surfaces *Surface Science* **1997**, *391*, L1217-L1223.

(58)   Ingemann-Hilberg, C.; Rudkjøbing, M. The 1s 2s States of Negative Hydrogen *Astrophys Space Sci* **1970**, *6*, 101.

(59)   Rudkjøbing, M. The Shape of the 11s0 − 21p1 Fano Resonance in the H- Photo-Ionization Continuum *Journal of Quantitative Spectroscopy and Radiative Transfer* **1973**, *13*, 1479-1501.

(60)   Bunge, C. F.; Galán, M.; Jáuregui, R.; Vivier Bunge, A. Systematic Search of Excited States of Negative Ions Lying above the Ground State of the Neutral Atom *Nuclear Instruments and Methods in Physics Research* **1982**, *202*, 299-305.